P4.9 FORMATION, EVOLUTION AND DECAY OF A SHEAR FLOW INSTABILITY IN THE STABLE NOCTURNAL BOUNDARY LAYER

Rob K. Newsom*, *CIRA, Colorado State University, Fort Collins, CO, USA*
Robert M. Banta, *Environmental Technology Laboratory/NOAA, Boulder, CO, USA*
Yelena Pichugina, *CIRA, Colorado State University, Fort Collins, CO, USA*

1. INTRODUCTION

This study investigates an apparent shear flow instability observed in a stably stratified boundary layer on 21 October 1999 during the Cooperative Atmosphere-Surface Exchange Study (CASES-99) in south-central Kansas. A scanning coherent Doppler lidar captured the velocity structure and evolution of a short-lived instability, and high-rate in-situ sensors mounted on a nearby 60-m tower, and on six surrounding 10-m towers provided wind and temperature data.

Wave activity was observed between 0030 and 0100 UTC, 21 October, 1999 (1930 to 2000 local time, 20 October, 1999). This occurred shortly after sunset during an evening transition period as a nocturnal surface-based inversion developed. The flow aloft (>100 m AGL) exhibited quasi-periodic fluctuations in wind speed. The time scales of these fluctuations were on the order of several 10s of minutes. Time series of low-level jet (LLJ) height exhibited significant fluctuations from 0100 to 0300 UTC (Banta et al. 2002). The event studied here occurred shortly before a LLJ structure was detected. The fluctuating flow aloft modulated the vertical shear below 100 m AGL, and evidently produced conditions conducive to the formation of shear instability within the surface-based inversion layer. This study focuses on a characterization of the observed wave event using Doppler lidar and in-situ tower data.

2. INSTRUMENTATION

Poulos et al. (2002) provides a comprehensive description of the CASES-99 field program and the instrumentation. The current study uses data from a Doppler lidar and in-situ tower sensors. Figure 1 displays a map of the CASES-99 main site and indicates the locations of instruments used in this study.

The NOAA High-Resolution Doppler Lidar (HRDL) is a scanning coherent Doppler lidar which operates at a wavelength of 2μm (Grund et al. 2001; Wulfmeyer 2000). HRDL measures range-resolved profiles of aerosol backscatter and radial velocity v_r, i.e. the component of velocity parallel to the beam.

The main 60-m tower was located about 1.45 km north of HRDL (see Fig 1). On the main 60-m tower wind measurements were provided by sonic and prop-vane anemometers, deployed at 5-m intervals. Sonic anemometers were sampled at 20 Hz, and the prop-vane anemometers were sampled at 1 Hz. Thirty-four thermocouples (Sun et al. 2002) were installed at 32 levels on the main tower and on two nearby 10-m towers. This provided temperature measurements with an average vertical resolution of 1.8 m. Thermocouples were sampled at 5 Hz.

Six 10-m towers were placed surrounding the main 60-m tower as shown in Fig 1. Instruments on each of the 10-m towers included, among others, sonic anemometers at the 5-m levels, and temperature sensors at the 2-m levels.

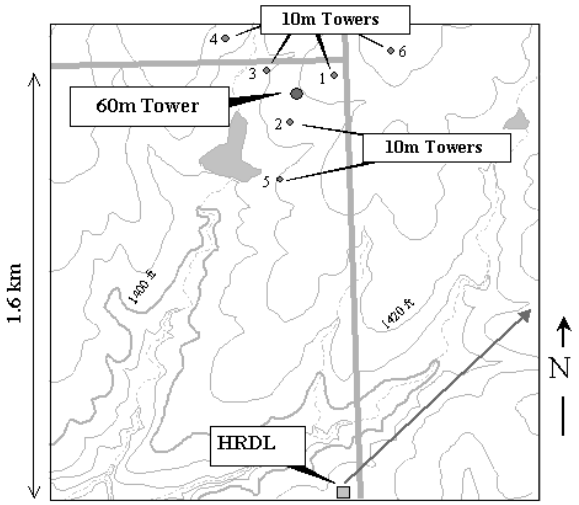

Figure 1 CASES-99 main site showing the location of HRDL relative to the main 60-m tower. The approximate locations of six 10-m towers or stations are also indicated. Stations are numbered one through six as indicated. The gray arrow originating from HRDL indicates the orientation of the vertical-slice scan that was performed between 0021 and 0038 UTC, 21 October 1999. The contour interval is 3.048 m (10 ft).

3. LIDAR OBSERVATIONS

Between 0021 and 0038 UTC, 21 October 1999, HRDL performed a series of vertical-slice scans, in which the laser beam was continuously swept through elevation angles θ_{lidar} from 0^o to 20^o at a fixed azimuth angle of $\phi_{lidar} = 50^o$. The six panels in Fig 2 display vertical cross sections of the horizontal velocity v_h field parallel to the scan plane. Each panel represents one scan or sweep in the vertical plane. Each scan required approximately 20 s to complete. Positive radial

* *Corresponding author address*: Dr. Rob K. Newsom, NOAA/ETL R/ET2, 325 Broadway, Boulder, CO, USA 80305-3328; e-mail: rob.k.newsom@noaa.gov.

velocities v_r indicate flow away from the lidar. The component of horizontal velocity projected into the plane of the scan , v_h , was computed by dividing the radial velocity by the cosine of the elevation angle, i.e. $v_h \approx v_r / \cos\theta_{lidar}$. This approximation is reasonable if the horizontal velocities are much larger than the vertical velocities and the elevation angles are small. For the scans shown in Fig 2 the maximum elevation angle was 20°.

Figure 2 indicates a general flow away from the lidar. Horizontal velocities near the surface were approximately 2ms^{-1}, and at z~150 m AGL the horizontal velocities were just over 8 ms^{-1}.

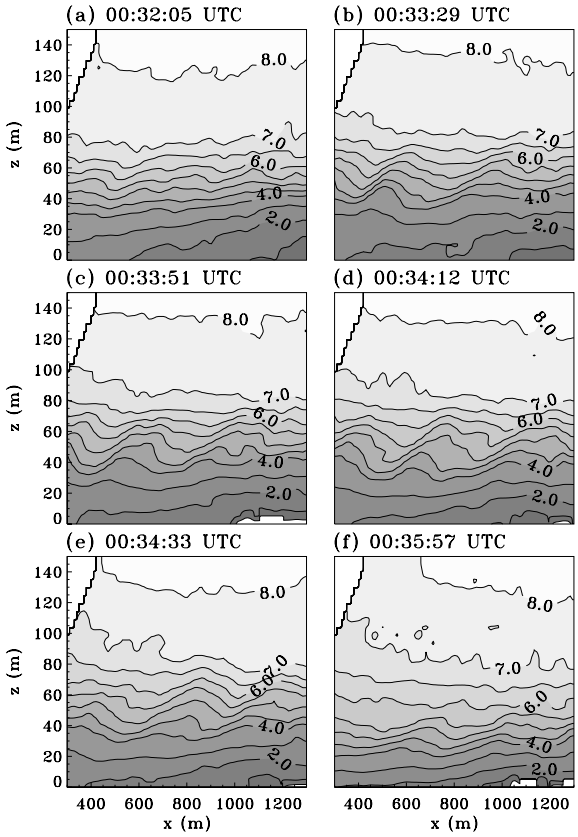

Figure 2 Sequence of HRDL vertical-slice scans of v_h from 21 October 1999. The horizontal scale represents range from the lidar, and contour labels are in ms^{-1}.

Panels (a) and (f) in Fig 2 show the flow structure before and after the wave event. Panels (b) through (e) show four sequential scans during the period of wave activity. This sequence of scans clearly show wave propagation away from the lidar. The wave-like motion was short-lived and persisted for less than three minutes (from roughly 0033 to 0036 UTC).

The wave activity indicated in Fig 2 occurred during a period in which the wind speed aloft (>100 m AGL) exhibited quasi-periodic fluctuations. Figure 3a displays a time-height cross-section of v_h at a horizontal range of 500 m from the lidar for the entire scan sequence (from 0021 to 0038 UTC). Figure 3b displays the corresponding values of $\partial v_h / \partial z$. We note that the time resolution of Fig 3 is not sufficient to resolve the wave fluctuations shown in Fig 2.

Figure 3a shows that from 0029 to 0032 UTC, v_h increased above roughly 50m AGL. During this same period v_h decreased slightly below 30 m AGL. This resulted in relatively strong vertical shear, $\partial v_h / \partial z$ between 20 m and 60 m AGL from 0031 to 0033 UTC. This is the period during which the waves first appeared. These observations suggest that the apparent shear flow instability was caused by both an acceleration of the flow aloft, and a slowing of the flow near the surface. The net result was the development of an inflection point elevated from the surface.

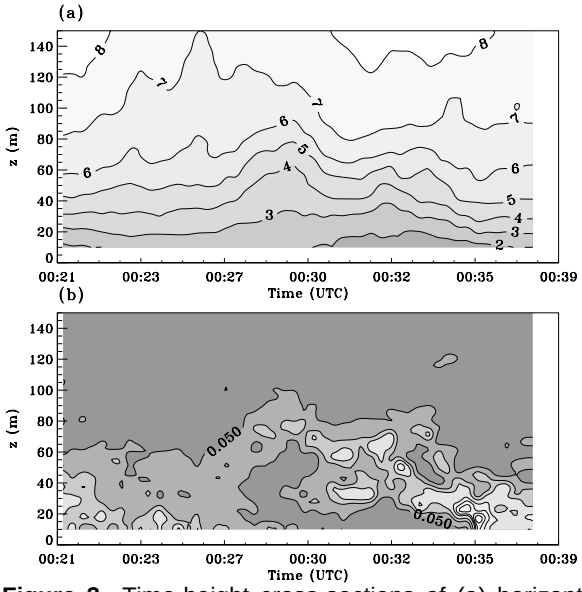

Figure 3 Time-height cross-sections of (a) horizontal winds v_h , and (b) vertcial shear $\partial v_h / \partial z$ from HRDL scan data. In (a) contour labels are in ms^{-1}. In (b) contour labels are in s^{-1}.

3.1 *Wave Properties*

The spatially and temporally resolved lidar measurements provide a means of estimating wave properties directly (e.g. wavelength and phase speed). Vertical profiles of horizontally averaged v_h variance indicate that the height of maximum wave amplitude occurred at about 47 m AGL between 0033 and 0034 UTC. However, we note that the lidar data also indicates a slight reduction in the height of maximum wave amplitude with time.

The lidar scan plane was likely not oriented precisely parallel to the direction of wave propagation. However, the misalignment between the scan azimuth and the propagation direction is probably not terribly

significant. Nevertheless, we will refer to the wavelength and phase speed as determined from the lidar data as the apparent wavelength λ_{lidar} and the apparent phase speed c_{lidar}, respectively. The true wavelength λ and phase speed c are related to λ_{lidar} and c_{lidar} by

$$\lambda_{lidar} = \lambda / \cos(\phi - \phi_{lidar})$$

and

$$c_{lidar} = c / \cos(\phi - \phi_{lidar}),$$

where ϕ is the azimuth of the wave propagation direction and ϕ_{lidar} is the azimuth of the lidar scan. From the lidar scan data shown in Figs 2b through 2e, λ_{lidar} was estimated to be $\lambda_{lidar} = 334$ m. The apparent phase speed c_{lidar} was estimated from a cross correlation analysis of v_h between successive scans at the height of maximum wave amplitude, 47m. The result of this analysis gave $c_{lidar} = 3.24\ \mathrm{ms}^{-1}$. Thus, relative to sensor fixed to the Earth frame, the lidar observations imply a wave frequency of

$$f = \frac{c}{\lambda} = \frac{c_{lidar}}{\lambda_{lidar}} = \frac{3.24\ \mathrm{ms}^{-1}}{334\ \mathrm{m}} = 0.0097\ \mathrm{Hz},$$

corresponding to a wave period of 103 s.

4. TOWER AND STATION OBSERVATIONS

The lidar observations showed that the wave activity occurred at heights accessible by sensors on the main 60-m tower. In order to corroborate the lidar observations, time series from anemometers and thermocouples on the main 60-m tower were examined for the presence of coherent fluctuations.

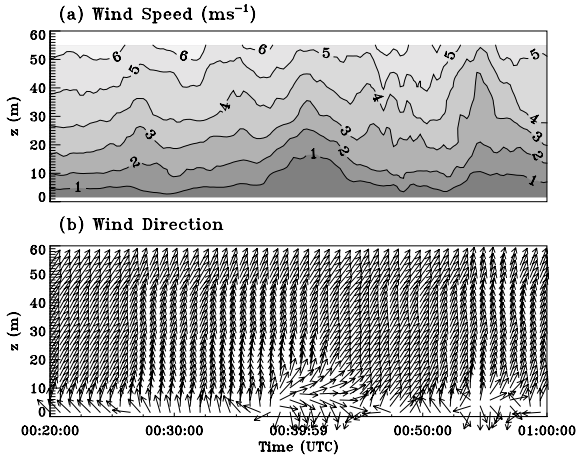

Figure 4 (a) Wind speed, and (b) wind direction from sonic and prop vane anemometers on the main tower.

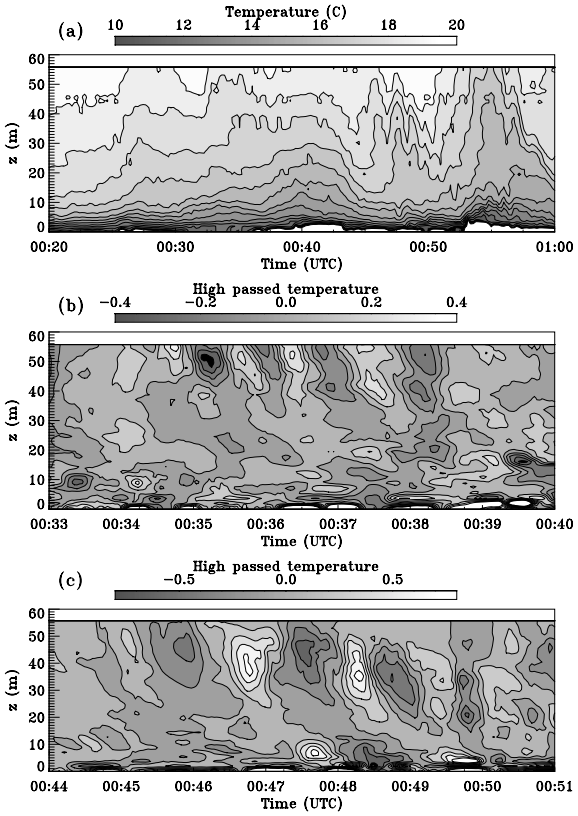

Figure 5 (a) Time-Height cross-section of thermocouple temperature, (b) high-pass filtered thermocouple data from 0033 to 0040 UTC, and (c) high-pass filtered thermocouple data from 0044 to 0051 UTC.

Figure 5a shows a time-height cross-section of thermocouple temperature for the period from 0020 to 0100 UTC. Figure 4 displays time-height cross-sections of wind speed (Fig 4a) and wind direction (Fig 4b) for the same period. Below roughly 20 m AGL there is a gradual cooling to about 0040 UTC. This is followed by a period of warming at the lower level and then significant cooling again beginning shortly after 0050 UTC. Periods of cooler air temperature correspond to periods of reduced wind speed (Fig 4a) and dramatic shifts in the wind direction (Fig 4b) at the lowest tower levels. From about 0045 to 0051 UTC there is considerable wave-like activity in the thermocouple temperature between 20 m and 50 m AGL. Additionally, the wind speeds (Fig 4a) also show some wave-like fluctuations during this period.

In order to better detect periods of wave activity a high-pass filter was applied to suppress fluctuations with periods longer than 4 min in time series from individual thermocouples. A close examination of the high-pass filtered thermocouple data reveals two periods of wave-like activity. Figure 5b displays a time-height cross-section of high-pass filtered thermocouple data for the first period of wave activity. Coherent fluctuations are evident from approximately 0034:30 to 0038 UTC above

the 40-m level. A second period of larger amplitude coherent fluctuations is shown in Fig 5c. This wave activity started at roughly 0046 UTC and persisted for approximately 4 min. As indicated in Fig 5c there is a noticeable downward propagation of the waves associated with the second event.

Estimates of wave frequencies or periods can be made from a visual inspection of the high-pass filtered thermocouple data shown in Figs 5b and 5c. From Fig 5b the wave period of the first event was estimated to be 50 s. From Fig 5c the wave period of the second event was estimated to be 90 s.

As previously mentioned two periods of lower wind speeds near the surface coincide with cooler surface temperatures and dramatic changes in wind direction. These periods occur just before and just after the second wave event observed in the thermocouple data.

In an effort to understand the mechanisms responsible for the strong wind direction shifts observed in Fig 4b, animations of wind vectors at 5 m AGL and temperature at 2 m AGL were generated from the network of stations (see Fig 1). These animations clearly indicate that the second wind shift event occurred in response to a surge of colder air propagating from north to south. For the first wind shift event, it is difficult to estimate the propagation direction based on the animations because the disturbance did not appear to have a well defined front associated with it. However, the general behavior suggests that both surface wind shift events were caused by shallow density currents associated with drainage flow from the slightly higher terrain to the north (see Fig 1).

5. SUMMARY

This paper documented an apparent shear flow instability observed shortly after sun set on 21 October, 1999 at the CASES-99 main field site, near Leon, KS. Lidar observations suggest that the apparent short-lived shear flow instability was triggered by an increase in the vertical shear. Larger-scale fluctuations in wind speed aloft combined with weakening flow near the surface, apparently due to shallow density currents, created relatively strong shear between 20 and 70m AGL.

The lidar observed wave activity between 0033 and 0036 UTC with a frequency of about 100 s. Thermocouple data from the main 60-m tower indicated two periods of coherent oscillations. The first period of wave activity occurred between roughly 0034:30 and 0038:30 UTC; these waves had a period of about 50 s. The second wave event observed by the thermocouples occurred between roughly 0046 and 0049 UTC; these waves had a period of about 90 s.

The wave activity observed by the lidar and the first wave event observed by the thermocouples overlap in time, but the estimated wave frequencies disagree. The beginning of the second wave event observed by the thermocouples occurs about 13 min after the first appearance of waves in the lidar scan data. In that case there is better agreement between the lidar and thermocouple wave frequencies.

Interpretation of the tower measurements in the context of the lidar observations is complicated by the relatively large separation between the lidar scan plane and the tower. The distance from the minimum range of the lidar to the tower was approximately 1300 m (see Fig 1). Without more complete data coverage it is impossible to determine precisely how the wave events observed by the lidar and the tower sensors are related. Considering the distance between the lidar scan plane and the tower, the wave events are likely not directly connected to each other. Rather, animations of lidar data suggest that the larger-scale disturbances aloft produced regions of increased shear, which more or less propagated along with the disturbances. Unstable waves continually formed and dissipated in the high-shear regions.

Acknowledgements. Funding for analysis and field measurements was provided by the Army Research Office, and the Center for Geosciences/Atmospheric Research at Colorado State University. The National Science Foundation (Grant # ATM-9908453) also provided funding for the field measurements. The authors are indebted to Dr. J. Sun, S. Burns, and Dr. S. Oncley of NCAR for tower data. NCAR is sponsored by the National Science Foundation.

REFERENCES

Banta, R.M., R.K. Newsom, J.K. Lundquist, Y.L. Pichugina, R.L. Coulter, and L.D. Mahrt, 2002: Nocturnal low-level jet characteristics over Kansas during CASES-99. *Boundary-Layer Meteor.*, in press.

Grund, C.J., R.M. Banta, J.L. George, J.N. Howell, M.J. Post, R.A. Richter, and A.M. Weickmann, 2001: High-Resolution Doppler Lidar for boundary-layer and cloud research. *J. Atmos. Oceanic Technol.*, **18**, 376-393.

Poulos, G.S., W. Blumen, , D.C. Fritts, J.K. Lundquist, J. Sun, S. Burns, C. Nappo, R.M. Banta, R. Newsom, J. Cuxart, E. Terradellas, B. Balsley, M. Jensen, 2000: CASES-99: A comprehensive investigation of the stable nocturnal boundary layer. *Bull. Amer. Meteor. Soc.*, accepted.

Sun J., D. H. Lenschow, S. P. Burns, R.M. Banta, R.K. Newsom, R. L. Coulter, S. Frasier, T. Ince, C. Nappo, B. Balsley, M. Jensen, D. Miller, B. Skelly, J. Cuxart, W. Blumen, X. Lee, and X. Z. Hu, 2002: Intermittent turbulence associated with a density current passage in stable boundary layer. *Boundary-Layer Meteor.*, in press.

Wulfmeyer, V., M. Randall, W. A. Brewer, R. M. Hardesty, 2000: 2 μm Doppler lidar transmitter with high frequency stability and low chirp. *Opt. Lett.*, **25**, 1228-1230.